Published OnlineFirst April 13, 2010; DOI: 10.1158/0008-5472.CAN-09-4439

Cancer Research

Pseudopodial Actin Dynamics Control Epithelial-Mesenchymal Transition in Metastatic Cancer Cells

Jay Shankar[1], Anat Messenberg[1], Jackie Chan[1], T. Michael Underhill[1], Leonard J. Foster[2], and Ivan R. Nabi[1]

Abstract

A key cellular process associated with the invasive or metastatic program in many cancers is the transformation of epithelial cells toward a mesenchymal state, a process called epithelial to mesenchymal transition or EMT. Actin-dependent protrusion of cell pseudopodia is a critical element of mesenchymal cell migration and therefore of cancer metastasis. However, whether EMT occurs in human cancers and, in particular, whether it is a prerequisite for tumor cell invasion and metastasis, remains a subject of debate. Microarray and proteomic analysis of actin-rich pseudopodia from six metastatic human tumor cell lines identified 384 mRNAs and 64 proteins common to the pseudopodia of six metastatic human tumor cell lines of various cancer origins leading to the characterization of 19 common pseudopod-specific proteins. Four of these (AHNAK, septin-9, eIF4E, and S100A11) are shown to be essential for pseudopod protrusion and tumor cell migration and invasion. Knockdown of each of these proteins in metastatic cells resulted in reduced actin cytoskeleton dynamics and induction of mesenchymal-epithelial transition (MET) that could be prevented by the stabilization of the actin cytoskeleton. Actin-dependent pseudopodial protrusion and tumor cell migration are therefore determinants of EMT. Protein regulators of pseudopodial actin dynamics may represent unique molecular targets to induce MET and thereby inhibit the metastatic potential of tumor cells.
Cancer Res; 70(9); 3780–90. ©2010 AACR.

Introduction

Tumor progression is a complex process that invokes multimodal parameters that enable tumor cells to evade host defense mechanisms and to migrate and establish new colonies or metastases. Dynamic actin cytoskeleton remodeling and stabilization of *de novo* substrate contacts drive pseudopodial protrusion and represent the basic mechanism by which cells migrate (1). Pseudopodial protrusion, and the formation of related invadopodia, has long been associated with tumor cell migration and invasion (2, 3). Expression of regulators of local actin reorganization critical for pseudopod protrusion, such as Wiskott-Aldrich syndrome protein family proteins, the Arp2/3 complex, Eps 8, α-actinin, fascin, filamin, LIM-kinase/cofilin, and cortactin, are closely associated with tumor cell migration and invasion and overexpressed in various cancers (4, 5). Actin cytoskeleton regulators were also recently identified as critical determinants of lymphoma progression in a loss-of-function RNA screen of mouse tumor models (6). Increased expression of Arp2/3 and WAVE2 correlates with poor prognosis in breast and liver carcinomas underlining the relevance of actin-dependent membrane protrusion and pseudopodia formation in cancer progression (7, 8). Cytokine activation stimulates intracellular signaling pathways that regulate the local reorganization of the actin cytoskeleton at the leading edge and drive pseudopodial protrusion (9–11). Proteins required for pseudopodial extension may therefore represent potential therapeutic targets to suppress tumor cell invasion and metastasis.

A key cellular process associated with the invasive or metastatic program in many cancers is the transformation of epithelial cells toward a mesenchymal state, a process called epithelial to mesenchymal transition or EMT (12). EMT is associated with altered gene expression patterns resulting in the loss of E-cadherin and the breakdown of cell-cell junctions as well as the acquisition of a fibroblastic morphology including polarized actin cytoskeleton assembly into protrusive and invasive pseudopodial structures. Mesenchymal transition enables invasive cells to break away from the invasive front, switch from collective to individual migration/invasion programmes, and navigate through the extracellular matrix and into the vasculature (13–15). However, although EMT is closely associated with the formation of protrusive pseudopodial structures, the relationship between pseudopod formation and EMT has yet to be characterized.

Authors' Affiliations: [1]Department of Cellular and Physiological Sciences, Life Sciences Institute and [2]Centre for High-Throughput Biology and Department of Biochemistry and Molecular Biology, University of British Columbia, Vancouver, British Columbia, Canada

Note: Supplementary data for this article are available at Cancer Research Online (http://cancerres.aacrjournals.org/).

Corresponding Author: Ivan R. Nabi, Department of Cellular and Physiological Sciences, Life Sciences Institute, University of British Columbia, 2350 Health Sciences Mall, Vancouver, BC V6T 1Z3, Canada. Phone: 604-822-7000; Fax: 604-822-2316; E-mail: irnabi@interchange.ubc.ca.

doi: 10.1158/0008-5472.CAN-09-4439

Published OnlineFirst April 13, 2010; DOI: 10.1158/0008-5472.CAN-09-4439

Molecular characterization of purified pseudopodial domains of fibroblasts, neurons, and cancer cells has led to the characterization of various populations of pseudopod-enriched RNAs and proteins (16–21). However, a comprehensive analysis of the mRNA and protein composition of pseudopodia of metastatic human cancer cells has yet to be undertaken. We report here the transcriptome/proteome analysis of six metastatic human tumor cell lines and identify four tumor cell pseudopod–specific proteins (AHNAK, Septin-9, eIF4E, and S100A11) whose expression is critical for pseudopod protrusion, actin cytoskeleton dynamics, and tumor cell migration and invasion. Of particular interest, loss of each of these proteins reverses EMT in these highly metastatic cell lines and results in cell-cell interaction, expression of E-cadherin, and reduced migration and invasion. Molecular effectors required for actin cytoskeleton dynamics and pseudopodial protrusions are therefore critical regulators of EMT and metastatic progression.

Materials and Methods

Antibodies and reagents. Mouse E-cadherin (#610182), N-cadherin (#610920), and β-catenin (#610153) antibodies were from BD Transduction Laboratories; anti-mitochondrial-Hsp70 were from Affinity Bioreagents; and anti–β-actin were from Sigma. AHNAK, eIF4E, S100A11, septin 9, RPL23, PTMA, ρ disassociation inhibitor factor α (RDIF-α;), calsequestrin S, rhotekin G, UBE2V2, TPM4, HNRPL1, COTL1, and SET antibodies were from Novus Biologicals. Alexa488–, Alexa568–, and Alexa647–conjugated secondary antibodies and rhodamine- and Alexa568-conjugated phalloidin were from Molecular Probes. Reagents for real-time PCR were from Applied Biosystems; the RNA isolation kit was from Qiagen; and Lipofectamine 2000 was from Invitrogen. Validated ON-TARGET plus SMARTpool small interfering RNAs (siRNA) for human septin-9, S100A11, eIF4E, and AHNAK, control siRNAs, and siGLO Red were from Dharmacon.

Cell culture, pseudopod purification, Western blot, and immunofluorescence. Human MDA-231, MDA-435, DU145, HT1080, U251, and U87 cell lines were from the American Type Culture Collection. MDA-231, MDA-435, and DU145 were maintained in complete RPMI 1640 and HT1080, U251, and U87 in DMEM supplemented with 10% fetal bovine serum, 100 IU/mL penicillin, 100 μg/mL streptomycin, 2 mmol/L L-glutamine, and 25 mmol/L HEPES buffer at 37°C in a humid atmosphere (5% CO_2 and 95% air). Pseudopodial preparation, isolation, and protein extraction were as previously described (19). Western blots were done as previously described (22). For immunofluorescence, cells grown on glass coverslips or 1-μ pore filter units (Falcon) were fixed with 3% paraformaldehyde and antibody was labeled as previously described (17, 19). Images were collected with ×60 or ×100 planapochromat objectives (numerical aperture, 1.35) of an FV1000 Olympus confocal microscope. The number of actin-labeled protrusions on the bottom of the filter relative to Hoechst-labeled nuclei on the top of the filter was quantified per ×100 microscope field. Pearson's colocalization coefficient was used to quantify the overlap of the fluorescently

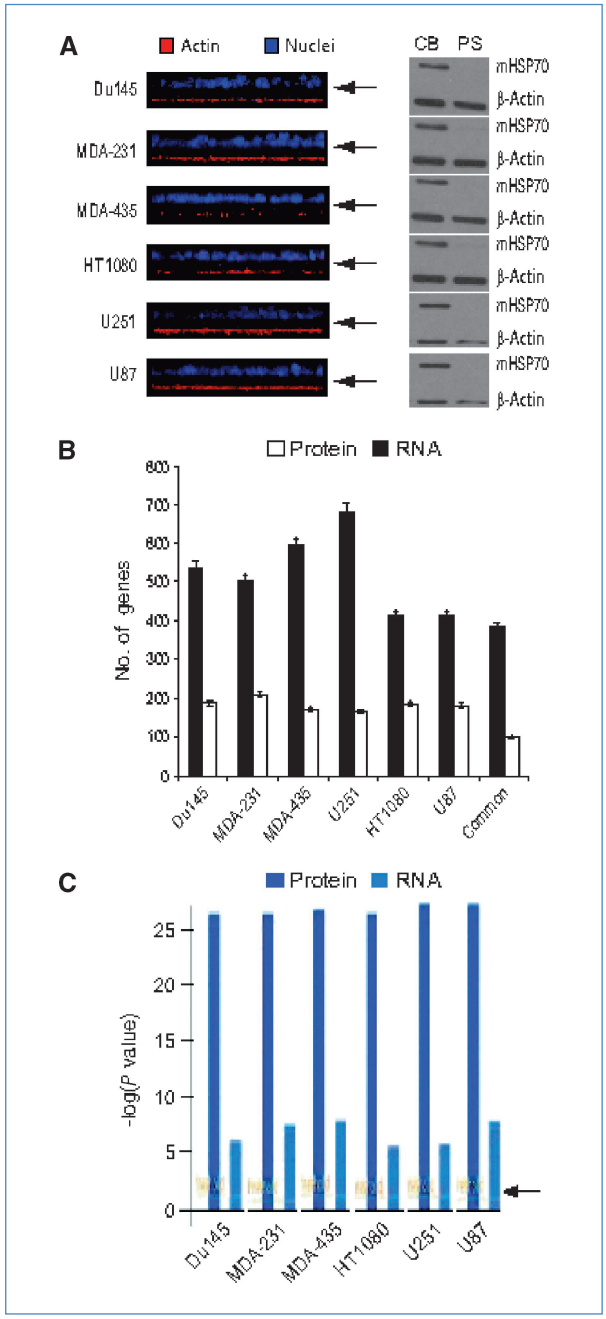

Figure 1. The transcriptome and proteome of tumor cell pseudopodia. A, metastastic prostate Du145, breast MDA-231 and MDA-435, fibrosarcoma HT1080, and glioma U251 and U87 cells were plated overnight on 1-μ pore filters and were F-actin labeled with rhodamine phalloidin (red) and nuclei with Hoechst (blue). Arrows, the position of the filter. Nuclei are not seen on the bottom of the filter and, to further assess the purity of the pseudopod fraction, cell body (CB) and pseudopod (PS) fractions, were purified and analyzed by Western blot for β-actin and mitochondrial HSP70 (mHSP70). Mitochondrial HSP70 is excluded from the pseudopod fraction in all six cell lines. B, number of pseudopodial mRNAs (black) and proteins (white) for each cell line and common to all cell lines were determined using the GENESPRING (GS) software. C, the cancer relevance of the cohorts of pseudopodial mRNA (light blue) and protein (dark blue) was determined using INGENUITY network analysis. Arrow, the threshold for significance ($P < 0.05$).

Published OnlineFirst April 13, 2010; DOI: 10.1158/0008-5472.CAN-09-4439

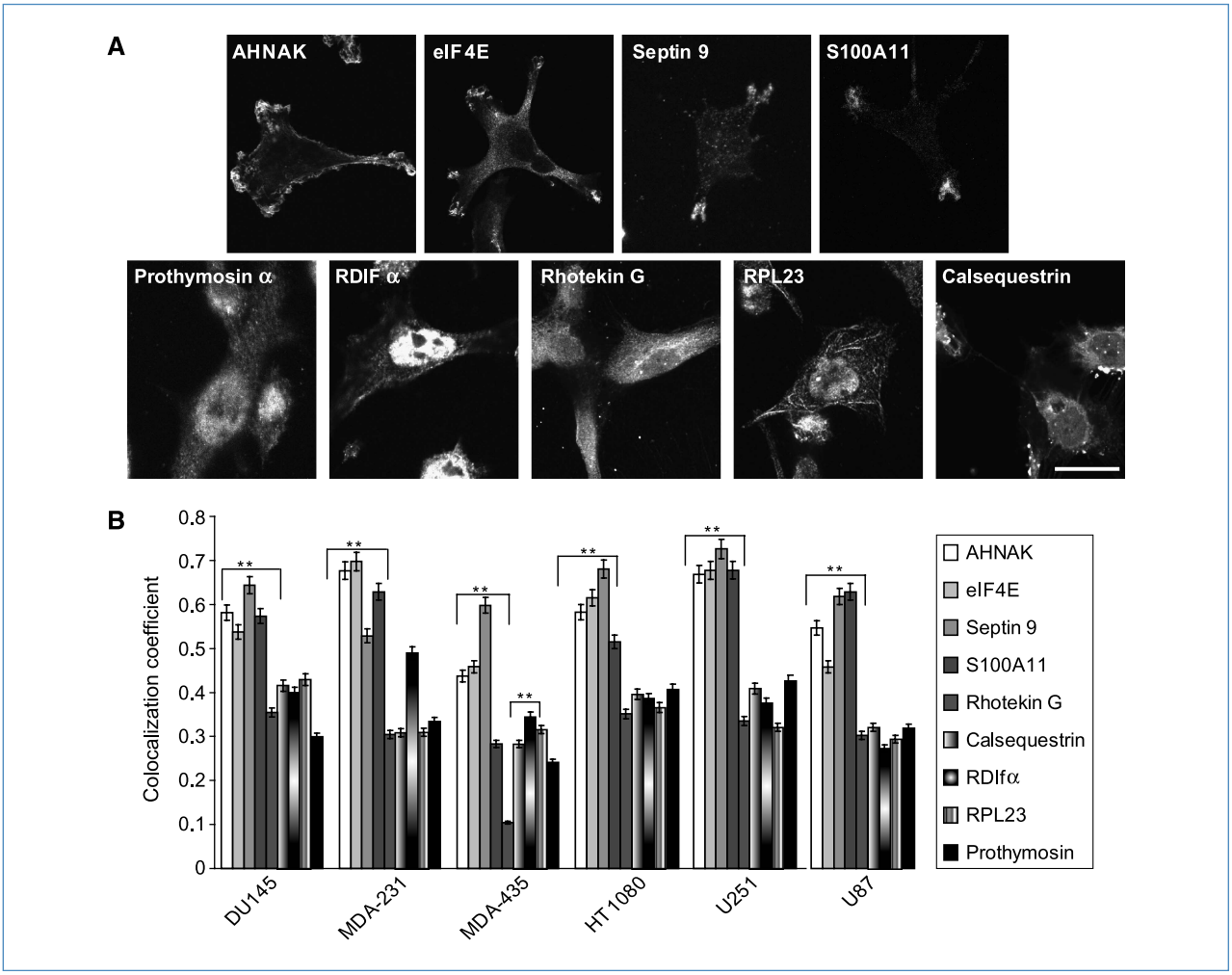

Figure 2. Pseudopod localization of identified proteins. A, metastatic Du145, MDA-231, MDA-435, HT1080, U251, and U87 cells plated overnight on coverslips were immunofluorescently labeled with antibodies against AHNAK, eIF4E, S100A11, septin 9, RPL23, PTMA, RDIF-α, calsequestrin S, and rhotekin G. AHNAK, eIF4E, S100A11, and septin 9 were concentrated in the pseudopodia compared with the other proteins. Images are from MDA-231 cells. B, colocalization coefficient for each protein was determined relative to actin and *P* value calculated relative to cell body localized rhotekin G (**, $P < 0.001$; *, $P < 0.05$). Scale bar, 10 μm.

labeled pseudopod proteins with actin-dense pseudopodial domains (ImagePro, Media Cybernetics).

Real-time PCR and siRNA. RNA was isolated from pseudopod and cell body fractions of each cell line using the RNeasy Plus mini kit (Qiagen) and was reverse-transcribed using the High Capacity cDNA Reverse Transcription kit (Applied Biosystems). Gene expression was quantified using real-time quantitative polymerase chain reaction (qPCR) on an ABI 7500 Fast system with custom Taqman probes for each gene using Taqman Gene Expression Assays (Applied Biosystems). Relative expression was determined using a standard curve and gene expression normalized to 18S abundance. Two micrograms of control or targeted siRNAs were transfected with Lipofectamine 2000 (Invitrogen) following the manufacturer's protocol, and cells were grown for 48 hours before assessing gene knockdown by Western blotting.

Affymetrix gene array and mass spectrometry. Affymetrix microarray analysis was performed as previously described (17). Briefly, biotinylated complementary RNA was prepared from 100 ng of total RNA as per the Affymetrix GeneChip Technical Analysis Manual (Affymetrix) using the two-cycle target-labeling assay. Double-stranded cDNA was synthesized using SuperScriptII (Invitrogen) and oligo$(dT)_{24}$ primers. Biotin-labeled complementary RNA was prepared by cDNA *in vitro* transcription using the BioArray high yield RNA transcript labeling kit (Enzo Biochem) incorporating biotinylated UTP and CTP. RNA was labeled and microarrays were processed at the London Regional Genomics Centre (Robarts Research Institute, London, Ontario, Canada). Thirty-six Affymetrix Human Genome U133 plus 2.0 arrays (three pseudopod and three cell body fractions from six cell lines) were scanned with the Affymetrix GeneChip Scanner 3000 and signal intensities for genes were generated with GCOS1.2

Published OnlineFirst April 13, 2010; DOI: 10.1158/0008-5472.CAN-09-4439

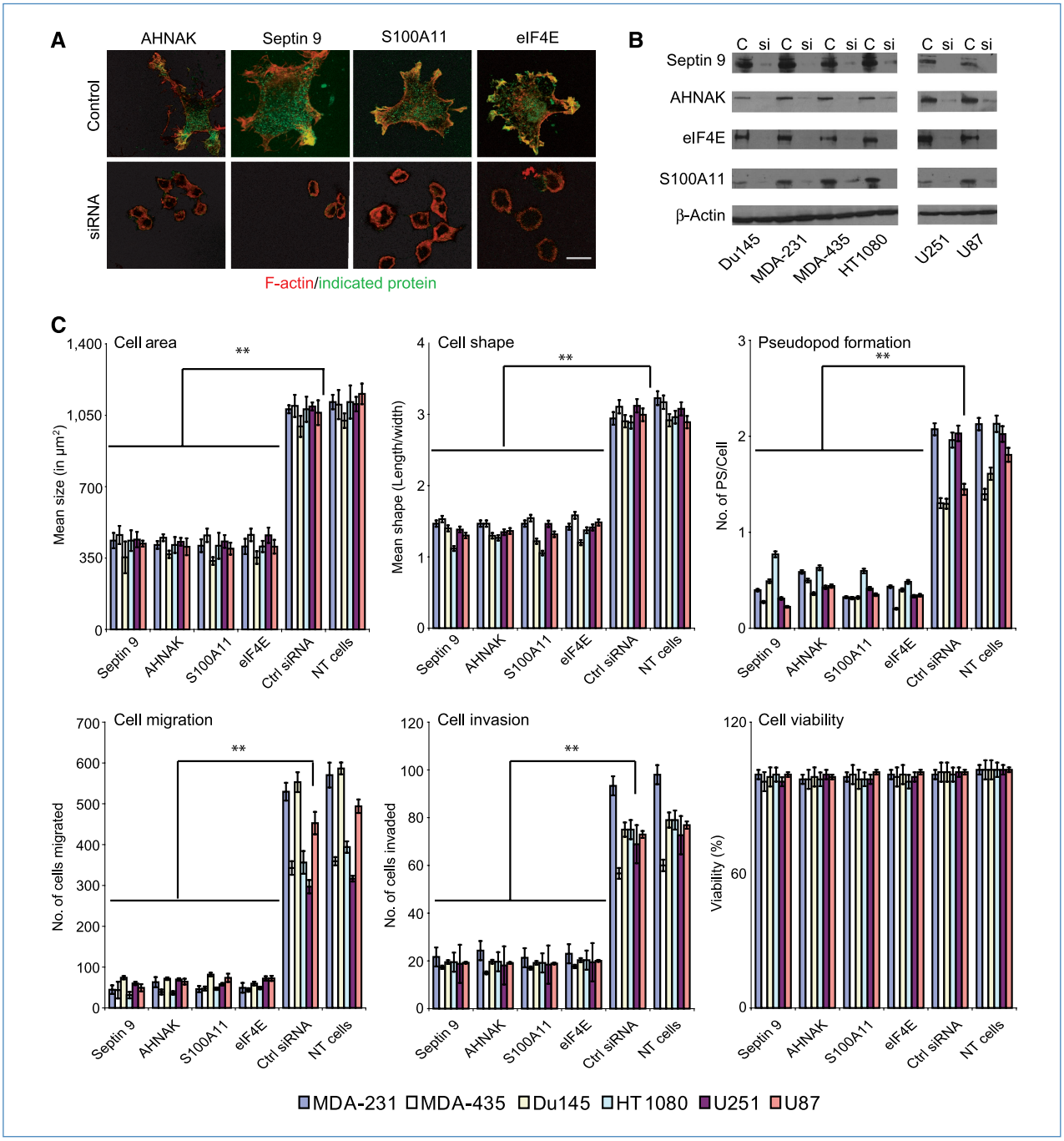

Figure 3. Pseudopod protein knockdown affects morphology, migration, and invasion of metastatic cancer cells. A, Du145, MDA-231, MDA-435, HT1080, U251, and U87 cells plated on coverslips overnight were transfected with control or specific siRNA against AHNAK, eIF4E, S100A11, and septin 9. After 48 hours, cells were immunofluorescently labeled with antibodies against AHNAK, eIF4E, S100A11, and septin 9 followed by appropriate secondary antibody (green) and rhodamine phallodin to label F-actin (red). Representative images from specific (bottom) and control (top) siRNA-treated MDA-231 cells are shown. B, lysates from cells transfected with control or specific siRNA against AHNAK, eIF4E, S100A11, and septin 9 were collected after 48 hours and Western blotted for AHNAK, eIF4E, S100A11, septin 9, and β-actin. C, cells plated on 96-well plates overnight were transfected with control or specific siRNA against AHNAK, eIF4E, S100A11, and septin 9. After 48 hours, transfected cells were labeled for F-actin (rhodamine phalloidin) and nuclei (Hoechst), and scanned using Cellomics ArrayScan VTi. The mean size of the transfected cells and control cells was determined using the Morphology Explorer Bioapplication Software Module (**, $P < 0.001$). For migration and invasion assays, siRNA-transfected cells were trypsinized after 48 hours and 3×10^4 cells were placed in Boyden chambers or Matrigel-coated invasion chamber, respectively ($n = 3$; columns, mean; bars, SEM). To assess pseudopodial protrusion, transfected cells were plated overnight on 1-μm pore filters and labeled for F-actin (rhodamine phalloidin) and nuclei (Hoechst), and the number of pseudopodia per cell quantified using the Image-Pro software. Cell viability of transfected cells was performed using WST-1 reagent. NT, nontransfected cells (**, $P < 0.001$). Scale bar, 5 μm.

Published OnlineFirst April 13, 2010; DOI: 10.1158/0008-5472.CAN-09-4439

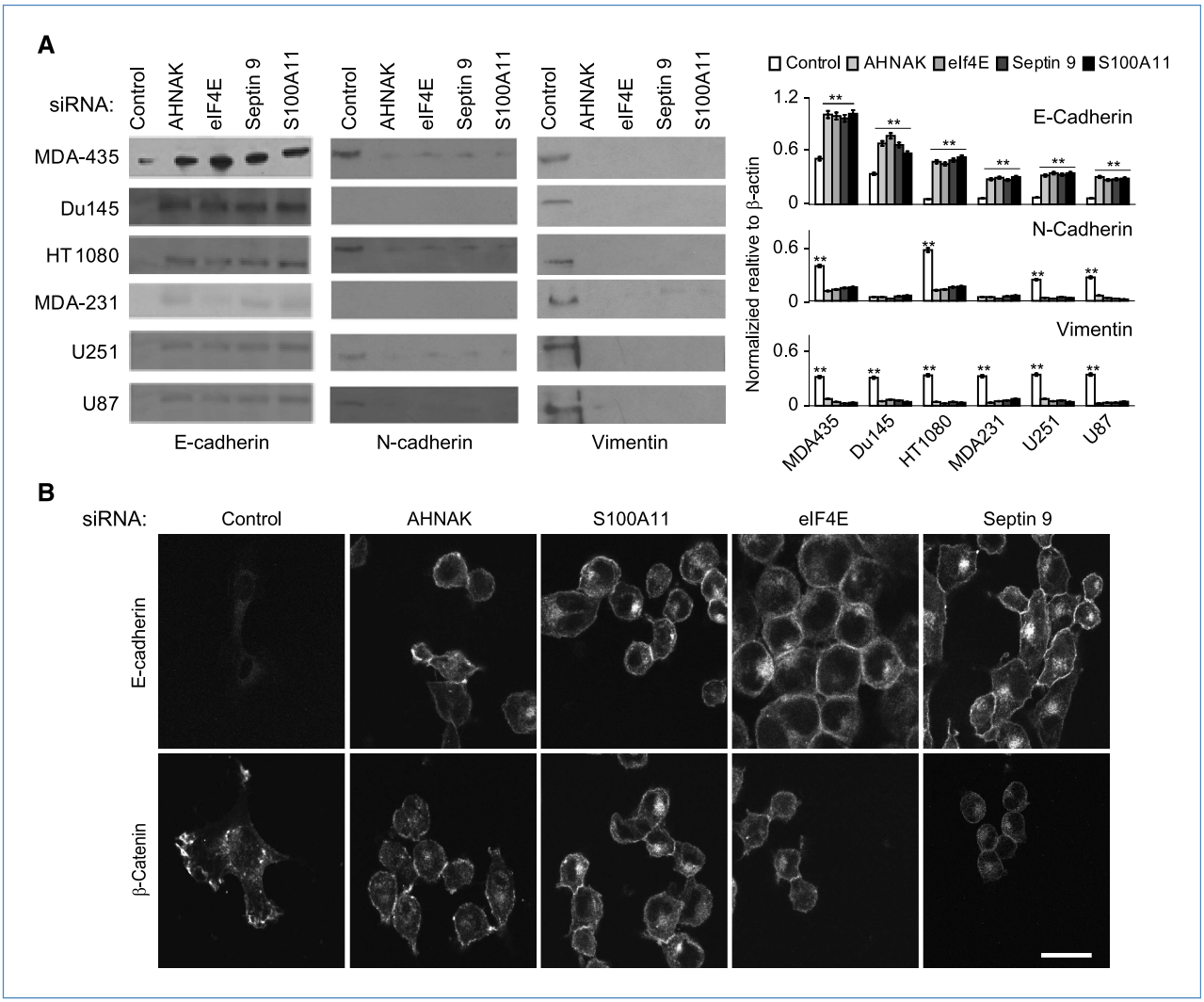

Figure 4. Pseudopod protein knockdown induces MET. A, lysates of Du145, MDA-231, MDA-435, HT1080, U251, and U87 cells transfected with control or specific siRNA against AHNAK, eIF4E, S100A11, and septin 9 were probed by Western blot for E-cadherin, N-cadherin, and vimentin. Bands were quantified by densitometry and normalized relative to β-actin (n = 3; columns, mean; bars, SEM). B, cells transfected with control or specific siRNA against AHNAK, eIF4E, S100A11, and septin 9 were immunofluorescently labeled for E-cadherin (top) or β-catenin (bottom). Representative images of MDA-231 cells show distribution of E-cadherin and β-catenin to the cell periphery in knockdown cells. Scale bar, 10 μm.

(Affymetrix) using the default values for statistical expression algorithm parameters, a target signal of 150 for all probe sets, and a normalization value of 1. GENESPRING was used to analyze the gene lists of mRNAs upregulated in tumor protrusions. Samples were prepared for mass spectrometry as previously described (23). Briefly, cell body and pseudopod fractions were extracted in 0.1 mol/L ammonium bicarbonate buffer (pH 8.0). Protein content was estimated using the Bradford reagent. Pseudopod proteins were solubilized by boiling in 1% deoxycholate/50 mmol/L Tris (pH 8.0) and were digested to peptides using trypsin before analysis by nanoflow liquid chromatography/tandem mass spectrometry using an LTQ-Orbitrap (ThermoFisher Scientific). The data discussed in this publication have been deposited in the National Center for Biotechnology Information Gene Expression Omnibus and are accessible through GEO Series accession number GSE20089. Gene lists of pseudopodial mRNAs and proteins were analyzed for disease relevance using the Ingenuity Pathways Analysis (Ingenuity Systems).

Migration, invasion, and cell proliferation. Forty-eight hours after siRNA transfection, cells were trypsinized, counted, and 3×10^4 cells were transferred to uncoated (migration) or Matrigel-coated (invasion) 8-μm cell culture inserts (BD Falcon) in medium containing 2% serum. The assembly was placed into 24-well plates containing complete medium. After 16 hours, nonmigrating and noninvasive cells were removed from the top of the filter with a cotton swab and migrating cells on the bottom of the filter were fixed with methanol acetone, stained with 0.5% crystal violet,

Published OnlineFirst April 13, 2010; DOI: 10.1158/0008-5472.CAN-09-4439

and counted. Cell proliferation assay was performed using the WST-1 reagent (Roche).

Cell spreading and actin microfilament turnover. Cell spreading and actin microfilament turnover were performed as previously described (24). Briefly, cells were grown in 96-well plates at 37°C for 24 hours, transfected with siRNA, fixed with 3% paraformaldehyde for 1 hour, and after three washes with PBS incubated with rhodamine phalloidin

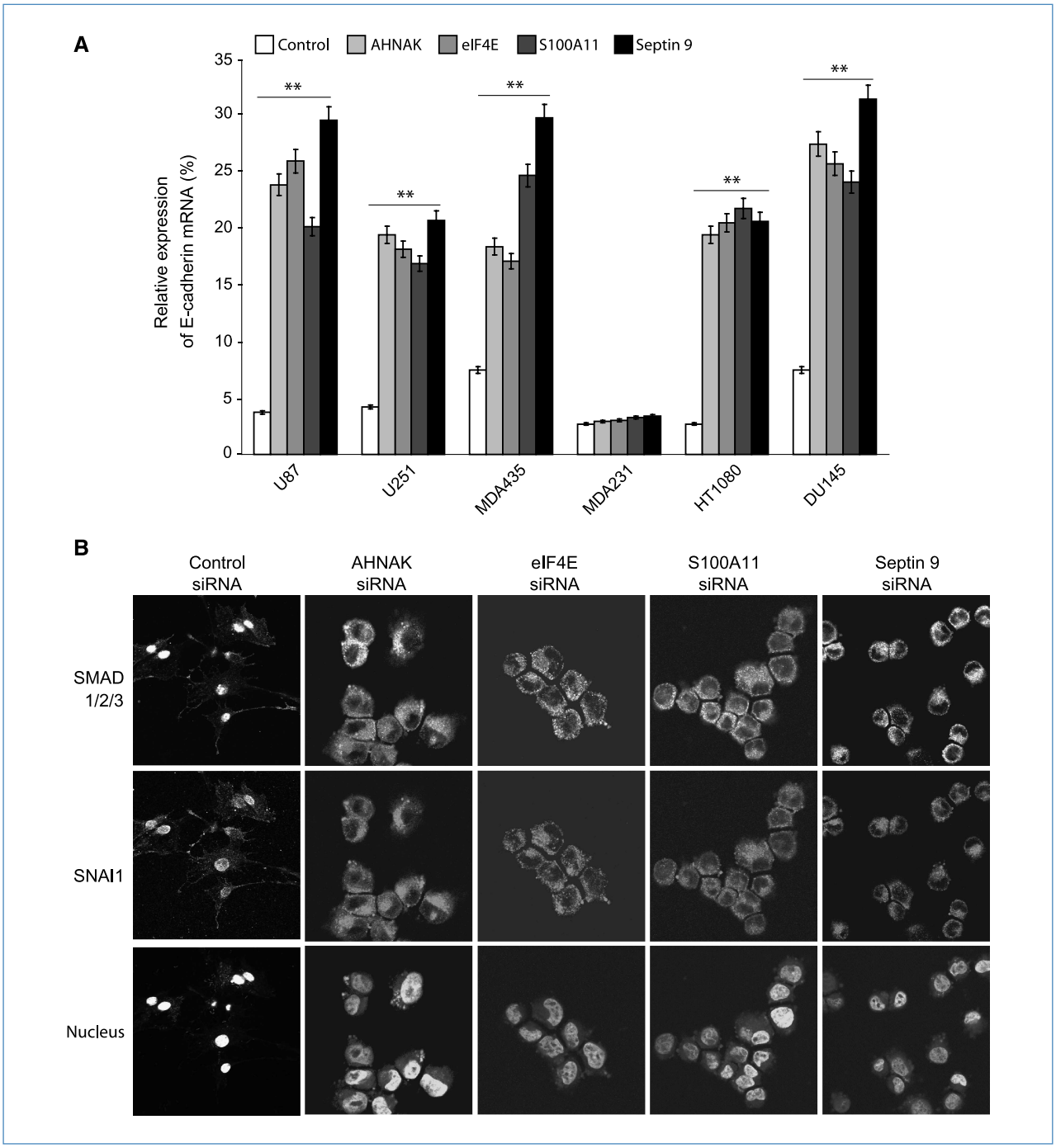

Figure 5. Pseudopod protein knockdown regulates E-cadherin mRNA expression and nuclear translocation of Smad and SNAI1. A, Du145, MDA-231, MDA-435, HT1080, U251, and U87 cells were transfected with control and siRNA against AHNAK, eIF4E, S100A11, and septin 9. After 48 hours, real-time PCR was performed to evaluate E-cadherin mRNA expression levels normalized and expressed as a percentage relative to 18s RNA. Knockdown of each protein increased E-cadherin mRNA expression levels in all cells except MDA-231. B, cells transfected with control and siRNA against AHNAK, eIF4E, S100A11, and septin 9 were fixed and labeled for Smad1/2/3 and SNAI1 followed by appropriate secondary antibodies and Hoechst to stain nuclei. Increased nuclear Smad1/2/3 and SNAI1 is observed in control cells relative to pseudopod protein knockdown cells. Scale bar, 10 μm.

Published OnlineFirst April 13, 2010; DOI: 10.1158/0008-5472.CAN-09-4439

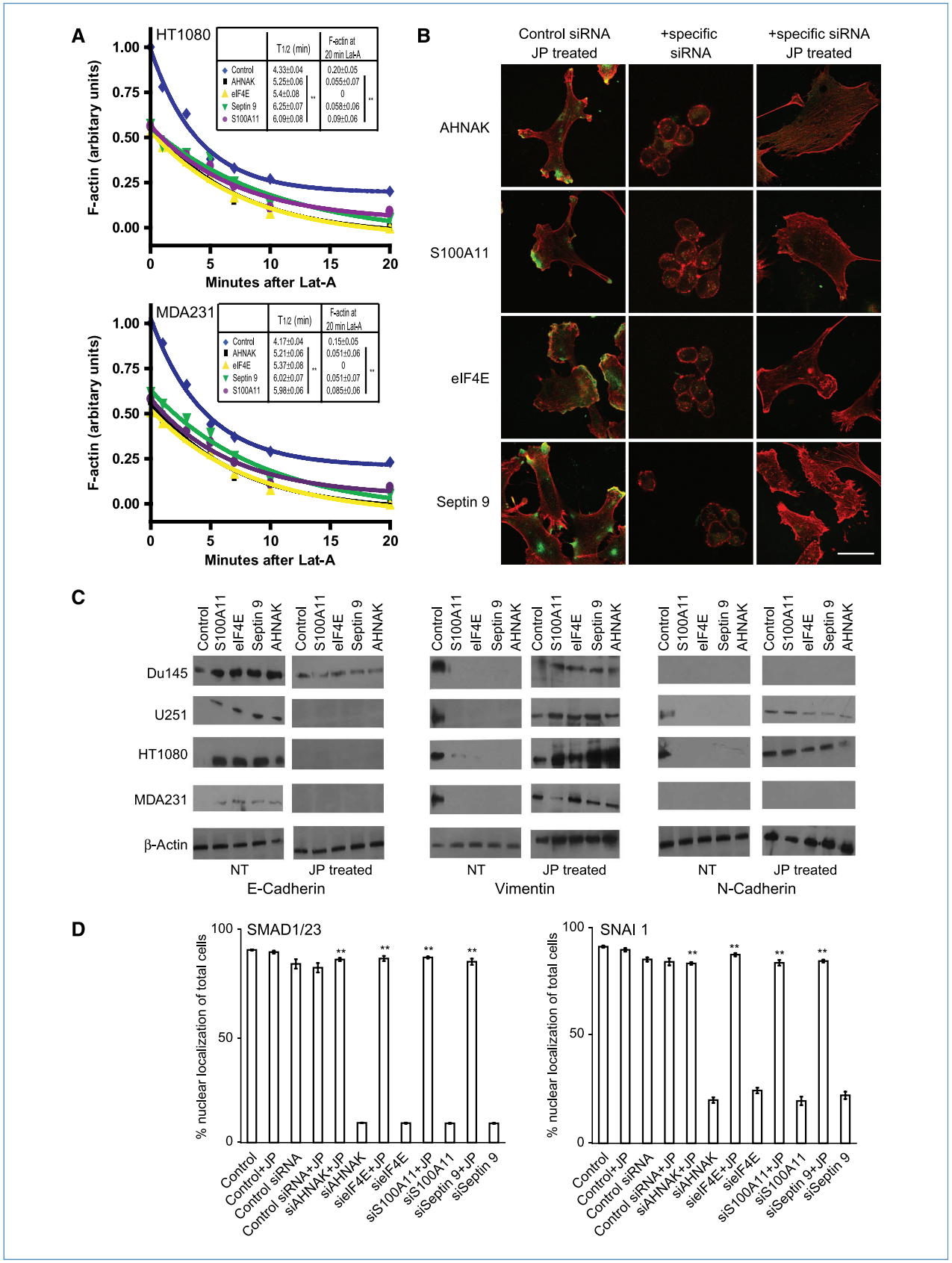

Published OnlineFirst April 13, 2010; DOI: 10.1158/0008-5472.CAN-09-4439

(1:500) and Hoechst (1:100) in the presence of 0.2% Triton X-100 for 30 minutes at room temperature. For actin microfilament turnover, cells were treated for 1 to 20 minutes with 0.5 μmol/L latranculin A, an actin monomer–binding drug that renders the monomers incompetent for filament formation, fixed with 3% paraformaldehyde for 15 minutes at room temperature, and labeled with Alexa 568–conjugated phalloidin [filamentous actin (F-actin)] and Hoechst stain (nucleus). Cells were scanned with a ×10 objective, identified by nuclear stain, and either cell area or phalloidin intensity was quantified using the Morphology Explorer Bioapplication software module of a Cellomics ArrayScan VTi. Data are means ± SEMs.

Jasplakinolide treatment. Cells were transiently transfected with siRNA and 22 to 24 hours (22 h for U251, and 24 h for MDA231, HT1080, and Du145) posttransfection and treated with different optimized jasplakinolide concentrations (U251, 50 nm; MDA231, 100 nm; HT1080/Du145, 150 nm) for 2 hours. Targeted protein knockdown was assessed by Western blot and F-actin distribution by immunofluorescence.

Results

Identification of pseudopod-localized gene products. Plating cells on 1-μm pore filters selectively allows the passage of actin-rich protrusions but not nuclei or the cell body through the filter pores (19, 25). Six metastatic tumor cell lines (breast MDA-231 and MDA-435, prostate Du145, fibrosarcoma HT1080, and glioma U251 and U87) that project actin-rich pseudopodia through 1-μm pore diameter polycarbonate filters were selected for further study (Fig. 1A). In all cases, nuclei were retained on the upper surface of the filter (Fig. 1A). Lysates were prepared from the upper cell body and lower pseudopod fractions, and as an indication of pseudopod fraction purity, Western blot analysis confirmed the presence of actin but not the mitochondrial Hsp70 protein in the pseudopod fraction from all six tumor cell lines (Fig. 1A). Pseudopod and cell body mRNA fractions were prepared from the six cell lines and analyzed by Affymetrix microarray analysis. Of the >23,000 genes analyzed, only 384 genes presented an absolute change >1.6-fold enrichment of mRNA expression in the pseudopod fraction relative to the cell body in all the cell lines (Supplementary Table S1; Fig. 1B). Proteomic analysis of the pseudopod fraction identified <200 proteins enriched in the pseudopodia of each cell line and 64 proteins common to all the tumor cell pseudopodia (Fig. 1B). Network analysis using the Ingenuity software showed that the cohort of pseudopodial mRNAs and proteins in each cell line as well as the common pseudopod-enriched cohorts were highly relevant to cancer (Fig. 1C).

We identified 19 pseudopod genes whose RNA was upregulated by microarray analysis in the pseudopod fraction of all six cell lines and was present by proteomic analysis in at least three cell lines (Supplementary Table S2). Of these, we chose desmoyokin (AHNAK nucleoprotein), prothymosin-α, ribosomal protein L23 (RPL23), septin-9, and calgizzarin (S100A11) for further study. We also included eukaryotic translation initiation factor 4E (eIF4E) that, although not among the pseudopod enriched mRNAs, was identified in the proteomic analysis of four cell lines (Supplementary Table S2) and has a well-characterized role in tumor progression and metastasis (26). As controls, we selected two cell body–enriched mRNAs (rhotekin G and calsequestrin S) and RDIF-α whose mRNA was pseudopod enriched but was not detected in the proteomic analysis.

We validated the pseudopodial distribution of mRNA and protein for the selected proteins by qPCR and Western blot, respectively (Supplementary Fig. S1A and B). Septin-9 and eIF4E mRNA were significantly enriched in the pseudopodia of six cell lines, and prothymosin α and S100A11 mRNA were enriched in the pseudopodia of two to three of the metastatic cell lines studied. Of the three cell body–enriched genes selected, only rhotekin G mRNA was confirmed to be cell body–enriched. However, at the protein level, clear enrichment of AHNAK, S100A11, septin 9, eIF4E, and prothymosin α was detected in pseudopod fractions of essentially all the cell lines studied. Similarly, calsequestrin, rhotekin G, and RDIF-α were all clearly enriched in the cell body fractions by Western blot (Supplementary Fig. S1B). Only RPL23 showed no clear distribution to either the cell body or pseudopod fractions.

The pseudopod distribution of the identified proteins was further assessed by immunofluorescent labeling of the six metastatic cell lines with specific antibodies and counterstaining F-actin with phalloidin. Representative labeling of MDA-231 cells (Fig. 2) shows that AHNAK, eIF4E, S100A11, and septin-9 were predominantly localized in the peripheral actin-rich pseudopodial domain. Prothymosin α,

Figure 6. Actin stabilization with jasplakinolide (JP) prevents MET induced by pseudopod protein knockdown. A, actin filament turnover of MDA-231 and HT1080 transfected with control or pseudopod protein–specific siRNAs was measured by quantifying the density of phalloidin-labeled F-actin per cell following treatment with 0.5 μmol/L Lat-A for 1, 3, 5, 7, 10, and 20 minutes. F-actin intensities were normalized to maximum and minimum values for each experiment. The half-life of F-actin depolymerization and residual F-actin densities after 20 minutes of Lat-A treatment are indicated (points, mean; bars, SEM; *P* values relative to controls unless otherwise indicated; *n* = 4). B, Du145, MDA-231, HT1080, and U251 cells were transfected with control or pseudopod protein–specific siRNAs. Before fixation, cells were treated with different concentrations of jasplakinolide for the times indicated in Materials and Methods and immunofluorescently labeled for AHNAK, eIF4E, S100A11, and septin 9 (green) and with rhodamine phallodin to label F-actin (red). Representative merged images for MDA-231 cells are shown. C, lysates of cells transfected with control or pseudopod protein–specific siRNA and treated or not with JP were Western blotted for E-cadherin, N-cadherin, and vimentin. JP treatment abrogated the effect of pseudopod protein knockdown on EMT marker expression. D, cells transfected with control or pseudopod protein–specific siRNA and treated or not with JP were immunofluorescently labeled for Smad1/2/3 or SNAI1 and Hoechst for nuclear staining. Nuclear distribution of Smad1/2/3 and SNAI1 was scored for control and specific siRNA-transfected cells (% positive nuclei; *n* = 4; columns, mean; bars, SEM). Scale bar, 10 μm.

Published OnlineFirst April 13, 2010; DOI: 10.1158/0008-5472.CAN-09-4439

RDIF-α, calsequestrin S, RPL23, and rhotekin G were distributed throughout the cell and exhibited reduced colocalization with F-actin (Fig. 2). As seen in Fig. 2B, AHNAK, eIF4E, S100A11, and septin-9 showed a higher colocalization coefficient relative to F-actin compared with the other proteins across all the cell lines, except for S100A11 in MDA-435 cells. In all cases, colocalization with F-actin was significantly elevated relative to rhotekin G/F-actin colocalization. Extension of this analysis to six other pseudopod-enriched proteins (UBE2V2, TPM4, HNRPL1, YWHAE, COTL1, and SET; Table 1) confirmed that all except HNRPL1 were enriched in tumor cell pseudopodia by Western blot and UBE2V2, TPM4, YWHAE, and COTL1 by immunofluorescence (Supplementary Fig. S2A and B). This domain-specific gene array and proteomic strategy across six metastatic cell lines of various tissue origins has therefore led to the identification of a cohort of pseudopod-enriched proteins of potential relevance to tumor cell migration and metastasis.

Pseudopod protein knockdown reduces cell spreading, migration, and invasion, and reverts EMT. To study the functional role of pseudopod-enriched proteins in tumor cell migration, we used a siRNA knockdown approach focusing on AHNAK, eIF4E, S100A11, and septin-9. Transient transfection of the six metastatic cell lines with target-specific siRNA resulted in the individual knockdown of protein level for AHNAK, eIF4E, S100A11, and septin-9 by >90% after 48 hours of transfection compared with control nontransfected and scrambled siRNA-transfected cells (Fig. 3A and B). Interestingly, knockdown of each of these four proteins did not affect the expression or distribution of the other three pseudopod-specific proteins that remained localized with the cortical actin cytoskeleton at the cell periphery (Supplementary Fig. S3). Individual knockdown of each of these four pseudopod-specific proteins resulted in dramatically reduced cell spreading and induced cell rounding relative to untransfected cells. Quantification using a Cellomics ArrayScan reader showed a >2-fold reduction in cell size and shape upon siRNA knockdown of all four proteins (Fig. 3A and C). The increased cell rounding was indicative of a loss of cellular protrusions and this was confirmed by the dramatic reduction in the number of actin-rich pseudopodia that protruded through 1-μm pores upon individual knockdown of the four pseudopod proteins (Fig. 3C), supporting a functional role for these proteins in pseudopod formation.

Reduced cell spreading and pseudopod formation upon knockdown of each of the four pseudopod-specific proteins suggested that these proteins also regulate cell migration and invasion. Indeed, knockdown of these proteins dramatically reduced migration in a Boyden chamber assay and invasion in Matrigel invasion chambers compared with cells transfected with control siRNA or nontransfected wild-type cells. However, no difference in viability of siRNA knockdown cells was detected (Fig. 3C). This result is consistent with a specific role for these pseudopodial proteins in tumor cell migration and invasion.

Of particular interest, knockdown of the four pseudopodial proteins was associated with *de novo* expression of E-cadherin that concentrated at sites of cell-cell interaction (Fig. 4) and redistribution of nuclear β-catenin from the nuclear region to peripheral junctional sites (Fig. 4). Knockdown was also associated with the loss of the mesenchymal markers N-cadherin and vimentin in all the cell lines except MDA-231 and DU145 cells that showed no expression of N-cadherin to begin with (Fig. 4). These results are consistent with a required role for each of these pseudopodial proteins in the induction of EMT. Real-time PCR also identified the increased expression of E-Cadherin mRNA upon knockdown of these four proteins in all the cell lines except for MDA-231 cells (Fig. 5A). Finally, Smad1/2/3 and SNAI1, transcription factors whose nuclear expression is associated with EMT (27), are nuclear localized in the metastatic cells studied but redistributed to the cytoplasm of knockdown cells, confirming the reversion of EMT upon knockdown of the four pseudopodial proteins (Fig. 5B).

Regulation of EMT by pseudopodial actin dynamics. Concentration of these proteins within actin-rich pseudopodia led us to test if knockdown of these proteins impacts on actin cytoskeleton dynamics. We treated control or siRNA-transfected MDA-231 and HT1080 cells with latrunculin-A (Lat-A), an inhibitor of actin polymerization, and measured the loss of F-actin density over time by phalloidin labeling. Knockdown cells for all four pseudopod-enriched proteins display reduced F-actin density, both before and after Lat-A treatment, and a slower loss of F-actin in the presence of Lat-A relative to nontreated or control siRNA-transfected cells (Fig. 6A). This suggests that each of these proteins function to regulate actin cytoskeleton dynamics.

Treatment of cells with the actin-stabilizing drug jasplakinolide prevented cell rounding and shrinking upon knockdown of pseudopod proteins (Fig. 6B). Importantly, in cells treated with jasplakinolide (U251, 50 nmol/L; MDA-231, 100 nmol/L; DU145, HT1080, 150 nmol/L) for the final 2 hours of siRNA treatment, pseudopod protein knockdown no longer induced the expression of E-cadherin or loss of expression of vimentin and N-cadherin (Fig. 6C). Jasplakinolide pretreatment further inhibited cytoplasmic translocation of the transcription factors Smad1/2/3 and SNAI1 (Fig. 6D). Actin cytoskeleton dynamics therefore plays a central role in the regulation of EMT by these pseudopodial proteins.

Discussion

Based on the fundamental requirement of pseudopod protrusion for tumor cell migration and metastasis, we used a combined transcriptomics and proteomics approach to identify 19 pseudopod-specific proteins in six metastatic cell lines of varying tumor origin, including breast, prostate, fibrosarcoma, and glioma. Knockdown of four pseudopod-enriched proteins, AHNAK, septin-9, eIF4E, and S100A11, resulted in pseudopod retraction, inhibition of cell migration and invasion, reduced actin cytoskeleton dynamics, and reversion of EMT. Our data define a direct link between pseudopodial actin dynamics and EMT, and suggest that targeting molecules crucial for pseudopod formation, such as those identified in

Published OnlineFirst April 13, 2010; DOI: 10.1158/0008-5472.CAN-09-4439

this study, might represent a means to revert EMT, inducing mesenchymal-epithelial transition (MET), and potentially inhibiting tumor cell metastasis.

Ingenuity pathway analysis of the cohorts of pseudopodial mRNAs and proteins in individual cell lines as well as those common to all six metastatic cell lines showed a high degree of cancer relevance (Fig. 1C). Expression of many of the 19 pseudopod-enriched proteins has been linked to various cancers. eIF4E has a well-established role in the progression of multiple cancer types and is actively being assessed as a therapeutic target for cancer therapy (26, 28). Expression of septin 9 is associated with malignant brain tumors (29). Higher levels of S100A11 expression are associated with colorectal cancer progression and invasion and metastasis of non–small cell lung cancer (30, 31). AHNAK was originally identified in neuroblastoma cancer cell lines; however, detailed study of its role in human cancers remains limited (32). Several other pseudopod-enriched proteins have also been reported to be associated with cancer including COTL1, YWHAE, ATP synthase, TPM4, SET, PTMA, and CNN2 (33–38). Importantly, many of the identified proteins (Table 1), such as COTL1, YWHAE, TPM4, CNN2, septin 9, AHNAK, S100A11, and eIF4E, have well-defined associations with the actin cytoskeleton (39–45). In addition, we also identified five ribosomal proteins (RPL11, RPL23, RPL6A, RPL13, and RPL27) that, together with pseudopodial enrichment of eIF4E, elongation factor α (46), and various other proteins associated with RNA translocation and protein translation (19), further supports actin-rich pseudopodia as sites of active protein translation. This domain-specific transcriptome and proteome analysis across multiple metastatic cancer cells of various tissue origins has therefore resulted in the identification of actin-associated proteins of potential cancer relevance.

Knockdown of each of these proteins reduces cellular F-actin content, actin turnover rate, and pseudopodial protrusion (Fig. 6), consistent with the established role of a dynamic actin cytoskeleton in pseudopod protrusion, as well as tumor cell migration and invasion. This suggests that they all act to promote pseudopod protrusion through a common mechanism associated with actin turnover and actin cytoskeleton remodeling. Although the specific relevance of each of the identified pseudopod-enriched proteins in cancer progression remains to be determined, this study underlies the critical importance of pseudopodial actin dynamics in the migratory and invasive phenotypes critical to tumor metastasis.

The fact that depletion of these proteins results in the reversion of EMT is of particular interest and links pseudopodial actin dynamics to transitions between epithelial and mesenchymal cell phenotypes. Indeed, the ability of actin stabilization with jasplakinolide to restore the expression of EMT markers after pseudopod protein knockdown suggests that a stable actin cytoskeleton is critical for EMT in cancer cells. Pseudopod protrusion is observed upon ErbB2-driven EMT in epithelial cells and may underlie increased invasiveness observed during EMT (47). E-cadherin binding to p120-catenin plays a fundamental role in the stability of epithelial cell-cell adhesions and regulates actin assembly required for the formation of membrane protrusions (48). However, although membrane protrusion formation is associated with EMT-driven cell invasion, there is to date no experimental evidence directly linking EMT to pseudopod formation (49). How pseudopodial actin dynamics are regulating EMT is unclear. However, the ability of a relatively short (2 hours) actin stabilization with jasplakinode to revert MET suggests that it is related not to transcriptional activity and gene regulation but rather to the regulation of local protein turnover that might be involved in the EMT process. That regulation of actin dynamics by both pseudopodial proteins and pharmacologic agents controls the expression of EMT markers defines for the first time, to our knowledge, the critical role of actin dynamics and pseudopodial protrusion and, therefore, the acquisition of a motile, migratory phenotype, on the induction of EMT.

Disclosure of Potential Conflicts of Interest

No potential conflicts of interest were disclosed.

Grant Support

The Cancer Research Society, Inc., Strategic Program in Genomics & Proteomics of Metastatic Cancer (http://src-crs.ca/). Mass spectrometry infrastructure used in this work was supported by the Canada Foundation for Innovation, the British Columbia Knowledge Development Fund and the Michael Smith Foundation through the BC Proteomics Network (BCPN). L.J. Foster is the Canada Research Chair in Organelle Proteomics and a Michael Smith Foundation Scholar.

The costs of publication of this article were defrayed in part by the payment of page charges. This article must therefore be hereby marked *advertisement* in accordance with 18 U.S.C. Section 1734 solely to indicate this fact.

Received 12/05/2009; revised 02/02/2010; accepted 02/18/2010; published OnlineFirst 04/13/2010.

References

1. Lauffenberger DA, Horwitz AF. Cell migration: a physically integrated molecular process. Cell 1996;84:359–69.
2. Guirguis R, Margulies I, Taraboletti G, Schiffmann E, Liotta L. Cytokine-induced pseudopodial protrusion is coupled to tumour cell migration. Nature (Lond) 1987;329:261–3.
3. Chen WT. Proteolytic activity of specialized surface protrusions formed at rosette contact sites of transformed cells. J Exp Zool 1989;251:167–85.
4. Le Clainche C, Carlier MF. Regulation of actin assembly associated with protrusion and adhesion in cell migration. Physiol Rev 2008;88:489–513.
5. Yamaguchi H, Condeelis J. Regulation of the actin cytoskeleton in cancer cell migration and invasion. Biochim Biophys Acta 2007;1773:642–52.
6. Meacham CE, Ho EE, Dubrovsky E, Gertler FB, Hemann MT. *In vivo* RNAi screening identifies regulators of actin dynamics as key determinants of lymphoma progression. Nat Genet 2009;41:1133–7.
7. Iwaya K, Norio K, Mukai K. Coexpression of Arp2 and WAVE2 predicts poor outcome in invasive breast carcinoma. Mod Pathol 2007;20:339–43.
8. Iwaya K, Oikawa K, Semba S, et al. Correlation between liver metastasis of the colocalization of actin-related protein 2 and 3 complex and WAVE2 in colorectal carcinoma. Cancer Sci 2007;98:992–9.

Published OnlineFirst April 13, 2010; DOI: 10.1158/0008-5472.CAN-09-4439

9. Cardone RA, Bagorda A, Bellizzi A, et al. PKA gating of a pseudopodial located RhoA/ROCK/p38/NHE1 signal module regulates invasion in breast cancer cell lines. Mol Biol Cell 2005;16:3117–27.
10. Vadnais J, Nault G, Daher Z, et al. Autocrine activation of the hepatocyte growth factor receptor/met tyrosine kinase induces tumor cell motility by regulating pseudopodial protrusion. J Biol Chem 2002; 277:48342–50.
11. Mouneimne G, DesMarais V, Sidani M, et al. Spatial and temporal control of cofilin activity is required for directional sensing during chemotaxis. Curr Biol 2006;16:2193–205.
12. Hay E, Zuk A. Transformations between epithelium and mesenchyme: normal, pathological, and experimentally induced. Am J Kidney Dis 1995;26:678–90.
13. Thiery JP. Epithelial-mesenchymal transitions in tumour progression. Nat Rev Cancer 2002;2:442–54.
14. Thiery JP, Sleeman JP. Complex networks orchestrate epithelial-mesenchymal transitions. Nat Rev Mol Cell Biol 2006;7:131–42.
15. Moreno-Bueno G, Portillo F, Cano A. Transcriptional regulation of cell polarity in EMT and cancer. Oncogene 2008;27:6958–69.
16. Beckner ME, Chen X, An J, Day BW, Pollack IF. Proteomic characterization of harvested pseudopodia with differential gel electrophoresis and specific antibodies. Lab Invest 2005;85:316–27.
17. Stuart H, Jia Z, Messenberg A, et al. RhoA/ROCK signaling regulates the delivery and dynamics of a cohort of mRNAs in tumor cell protrusions. J Biol Chem 2008;283:34785–95.
18. Poon MM, Choi SH, Jamieson CA, Geschwind DH, Martin KC. Identification of process-localized mRNAs from cultured rodent hippocampal neurons. J Neurosci 2006;26:13390–9.
19. Jia Z, Barbier L, Stuart H, et al. Tumor cell pseudopodial protrusions. Localized signaling domains coordinating cytoskeleton remodeling, cell adhesion, glycolysis, RNA translocation, and protein translation. J Biol Chem 2005;280:30564–73.
20. Cho SY, Klemke RL. Purification of pseudopodia from polarized cells reveals redistribution and activation of Rac through assembly of a CAS/Crk scaffold. J Cell Biol 2002;156:725–36.
21. Mili S, Moissoglu K, Macara IG. Genome-wide screen reveals APC-associated RNAs enriched in cell protrusions. Nature (Lond) 2008; 453:115–9.
22. Joshi B, Strugnell SS, Goetz JG, et al. Phosphorylated caveolin-1 regulates Rho/ROCK-dependent focal adhesion dynamics and tumor cell migration and invasion. Cancer Res 2008;68:8210–20.
23. Chan QW, Foster LJ. Changes in protein expression during honey bee larval development. Genome Biol 2008;9:R156.
24. Lagana A, Goetz JG, Cheung P, Raz A, Dennis JW, Nabi IR. Galectin binding to Mgat5-modified N-glycans regulates fibronectin matrix remodeling in tumor cells. Mol Cell Biol 2006;26:3181–93.
25. Nguyen TN, Wang HJ, Zalzal S, Nanci A, Nabi IR. Purification and characterization of β-actin-rich tumor cell pseudopodia: role of glycolysis. Exp Cell Res 2000;258:171–83.
26. Sonenberg N. eIF4E, the mRNA cap-binding protein: from basic discovery to translational research. Biochem Cell Biol 2008;86:178–83.
27. Lee JM, Dedhar S, Kalluri R, Thompson EW. The epithelial-mesenchymal transition: new insights in signaling, development, and disease. J Cell Biol 2006;172:973–81.
28. Graff JR, Konicek BW, Carter JH, Marcusson EG. Targeting the eukaryotic translation initiation factor 4E for cancer therapy. Cancer Res 2008;68:631–4.
29. Kim DS, Hubbard SL, Peraud A, Salhia B, Sakai K, Rutka JT. Analysis of mammalian septin expression in human malignant brain tumors. Neoplasia 2004;6:168–78.
30. Wang G, Wang X, Wang S, et al. Colorectal cancer progression correlates with upregulation of S100A11 expression in tumor tissues. Int J Colorectal Dis 2008;23:675–82.
31. Tian T, Hao J, Xu A, et al. Determination of metastasis-associated proteins in non-small cell lung cancer by comparative proteomic analysis. Cancer Sci 2007;98:1265–74.
32. Shtivelman E, Cohen FE, Bishop JM. A human gene (AHNAK) encoding an unusually large protein with a 1.2-microns polyionic rod structure. Proc Natl Acad Sci U S A 1992;89:5472–6.
33. Li DQ, Wang L, Fei F, et al. Identification of breast cancer metastasis-associated proteins in an isogenic tumor metastasis model using two-dimensional gel electrophoresis and liquid chromatography-ion trap-mass spectrometry. Proteomics 2006;6:3352–68.
34. Chang HJ, Lee MR, Hong SH, et al. Identification of mitochondrial FoF1-ATP synthase involved in liver metastasis of colorectal cancer. Cancer Sci 2007;98:1184–91.
35. Nakatsura T, Senju S, Ito M, Nishimura Y, Itoh K. Cellular and humoral immune responses to a human pancreatic cancer antigen, coactosin-like protein, originally defined by the SEREX method. Eur J Immunol 2002;32:826–36.
36. Cimino D, Fuso L, Sfiligoi C, et al. Identification of new genes associated with breast cancer progression by gene expression analysis of predefined sets of neoplastic tissues. Int J Cancer 2008;123: 1327–38.
37. Carlson SG, Eng E, Kim EG, Perlman EJ, Copeland TD, Ballermann BJ. Expression of SET, an inhibitor of protein phosphatase 2A, in renal development and Wilms' tumor. J Am Soc Nephrol 1998;9: 1873–80.
38. Tsai YS, Jou YC, Lee GF, et al. Aberrant prothymosin-α expression in human bladder cancer. Urology 2009;73:188–92.
39. Provost P, Doucet J, Stock A, Gerisch G, Samuelsson B, Radmark O. Coactosin-like protein, a human F-actin-binding protein: critical role of lysine-75. Biochem J 2001;359:255–63.
40. Tak H, Jang E, Kim SB, et al. 14-3-3ε inhibits MK5-mediated cell migration by disrupting F-actin polymerization. Cell Signal 2007;19: 2379–87.
41. Lin JJ, Eppinga RD, Warren KS, McCrae KR. Human tropomyosin isoforms in the regulation of cytoskeleton functions. Adv Exp Med Biol 2008;644:201–22.
42. Chacko AD, Hyland PL, McDade SS, Hamilton PW, Russell SH, Hall PA. SEPT9_v4 expression induces morphological change, increased motility and disturbed polarity. J Pathol 2005;206:458–65.
43. Benaud C, Gentil BJ, Assard N, et al. AHNAK interaction with the annexin 2/S100A10 complex regulates cell membrane cytoarchitecture. J Cell Biol 2004;164:133–44.
44. Zhao XQ, Naka M, Muneyuki M, Tanaka T. Ca(2+)-dependent inhibition of actin-activated myosin ATPase activity by S100C (S100A11), a novel member of the S100 protein family. Biochem Biophys Res Comm 2000;267:77–9.
45. Lindemann S, Tolley ND, Eyre JR, Kraiss LW, Mahoney TM, Weyrich AS. Integrins regulate the intracellular distribution of eukaryotic initiation factor 4E in platelets. A checkpoint for translational control. J Biol Chem 2001;276:33947–51.
46. Liu G, Grant WM, Persky D, Latham VM, Jr., Singer RH, Condeelis J. Interactions of elongation factor 1α with F-actin and β-actin mRNA: implications for anchoring mRNA in cell protrusions. Mol Biol Cell 2002;13:579–92.
47. Khoury H, Dankort DL, Sadekova S, Naujokas MA, Muller WJ, Park M. Distinct tyrosine autophosphorylation sites mediate induction of epithelial mesenchymal like transition by an activated ErbB-2/Neu receptor. Oncogene 2001;20:788–99.
48. Noren NK, Liu BP, Burridge K, Kreft B. p120 catenin regulates the actin cytoskeleton via Rho family GTPases. J Cell Biol 2000;150: 567–80.
49. Yilmaz M, Christofori G. EMT, the cytoskeleton, and cancer cell invasion. Cancer Metastasis Rev 2009;28:15–33.

AACR American Association for Cancer Research

Cancer Research

The Journal of Cancer Research (1916–1930) | The American Journal of Cancer (1931–1940)

Pseudopodial Actin Dynamics Control Epithelial-Mesenchymal Transition in Metastatic Cancer Cells

Jay Shankar, Anat Messenberg, Jackie Chan, et al.

Cancer Res 2010;70:3780-3790. Published OnlineFirst April 13, 2010.